RAPID NON-DESTRUCTIVE X-RAY DIFFRACTION INVESTIGATION OF POLISHED GREENSTONE TOOLS

ZÖLDKŐ TÍPUSÚ CSISZOLT KŐESZKÖZÖK GYORS RONCSOLÁS MENTES RÖNTGENDIFFRAKCIÓS VIZSGÁLATA

FERENC KRISTÁLY

Miskolc-Egyetemváros, 3515 Hungary

E-mail: askkf@uni-miskolc.hu

Abstract

During the research of polished stone tools we may frequently find rare, valuable and unique exemplars. These qualities in many cases are determined by the rock type the tool has been made from. Among Hungarian findings, high pressure metamorphic rock made tools are rare. These cannot be identified based on their macroscopic appearance, colour or texture. The precise mineralogical investigations needed for their identification can be made by X-ray diffraction. Since we have to deal with unique pieces, non-destructive technique must be applied. On a laboratory diffractometer this can be done with the use of Göbel mirror, in parallel beam geometry. With a scintillation detector measurement times up to 8 hours are necessary, but position sensitive detectors allow recording times of minutes. Our measurements were carried out with 15 minutes recording. Instrumental alignment and precision was tested with the use standards. Identification of rock forming components was possible with accuracy using Search/Match algorithm. Measurement times were reduced to even 1 minute, depending on measured surface and rock type. Our measurements revealed the existence of eclogite type omphacitic and jadeite bearing rocks, amphibolites and nephrites, chlorite schist and hornfels type contact metamorphite. According to our observations, textural features and orientation patterns can be extracted, if necessary.

Kivonat

A csiszolt kőeszközök kutatása során gyakran találkozunk ritka, értékes és egyedi példányokkal. Ezeket a tulajdonságokat sokszor a kőzet típusa határozza meg, amiből készült az eszköz. Magyarországi leletek között ritkák a nagy nyomású metamorfitokból készült balták és vésők. Makroszkópos megjelenésük, színük és szövetük alapján nehezen határozhatók meg. Az azonosításukhoz szükséges pontos ásványtani vizsgálatát röntgen diffrakcióval lehet végezni. Mivel egyedi példányokról beszélünk, roncsolásmentes eljárást kell alkalmazni. Laboratóriumi pordiffraktométeren ezt az eljárást Göbel tükörrel, párhuzamos nyaláb geometriában tudjuk elvégezni. Szcintillációs detektorral akár 8 órás mérésekre is szükség lehet, de helyzetérzékelő detektorral percek alatt elvégezhető a mérés. Vizsgálatainkat átlagosan 15 perces méréssel végeztük. A műszer beállításait és pontosságát standardokkal ellenőriztük. A kőzetalkotó ásványok azonosítását nagy pontossággal el tudtuk végezni a Search/Macth algoritmus alkalmazásával. Mintafelülettől és anyagtípustól függően 1 perces mérési időt is elegendőnek találtunk az azonosításhoz. A méréseink során eklogit típusú omfacitos és jadeites kőzeteket, amfibolitokat és nefriteket valamint kloritpalát és szaruszírt típusú kontakt metamorfitot azonosítottunk. Megfigyeléseink szerint, ha szükséges, szövet-szerkezeti, szöveti orientációs adatokat is ki tudunk nyerni.

KEYWORDS: NON-DESTRUCTIVE XRD, PYROXENITE, OMPHACITE SEARCH/MATCH, NEPHRITE, XRD

KULCSSZAVAK: RONCSOLÁSMENTES XRD, PIROXENIT, OMFACIT SEARCH/MATCH, NEFRIT, XRD

Introduction

X-ray diffraction investigations make the basis of materials science and related research fields since many decades. May we speak of single crystal, powder or micro diffraction, the structure (crystalline or not) of materials is mainly resolved by using X-rays. This is due to the elaboration of many laboratory scale instrument types and high performance laboratory X-ray sources. Perhaps the most widespread application is that of the Bragg-Brentano (or parafocusing) powder diffractometers, which gives the best resolution – intensity geometry (Brentano 1946). This is used to obtain data for crystal structure solution, quantitative mineralogical evaluation or simply identification of sample components. Powder diffractometers are also suitable for the investigation of "block" samples, if the means of sample surface quality and alignment requirements are satisfied (see metallurgical applications, Kocks et al. 2000). For a Bragg-Brentano diffractometer, this would mean a polished – planar surface, which can be adjusted at least with ± 0.01 mm to the sample height reference plane of the goniometer circle.

This problem was overcome by developing parallel beam geometry (Schuster & Göbel 1995), with X-

ray optical attachments such as a Göbel mirror (Deslates et al. 1997). This way, surface roughness and sample height error or displacement is not a problem (Holz et al. 2000), and measurements can be carried out on any solid material, that can be adjusted in the sample chamber of the apparatus. By this application the X-ray diffraction evolved into a totally non-destructive analytical method.

In archaeometry, we encounter frequently valuable objects that cannot be investigated by traditional analytical methods (e.g. powder diffraction, thin sections, and solution based chemical analysis). Non-destructive XRD is currently the only available technique to investigate properties related to crystalline structure of such materials. The Göbel mirror solution of Bruker AXS Ltd. has been applied in several archaeological cases in the last decade, for various artefacts (Duran et al. 2008), glasses, ceramics (Kristály & Kovács 2011) and even stone tools (Chiari et al. 1996). We also have investigated the reliability of this technique by using powder, micro powder and sliced specimens of various stone tools. As it was expected, identification of crystalline components is possible, even at accessory minerals level. But several major issues may lead to false identifications. One of these is preferred orientation of crystals (or grains) mainly of fibrous and platy minerals. Also the base line profile is highly influenced by the shape of analyzed surface, permitting erroneous amorphous phase observations. But one of the major setbacks is measurement time, which is required to be up to 8 hours in most cases. This issue can be partly overcome with the use of position sensitive detectors, which reduce measurement times even to 1/10, although sample surface alignment requires more attention.

As we can learn from papers dedicated to stone tool research (Gan et al. 2010, Giustetto et al. 2008), many analytical techniques are useful and applicable as non-destructive. Chemical information is easier to obtain in a non-destructive way, and even mineralogical information can be extracted e.g. by Raman microscopy (Smith & Gedron 1997), but crystallographic data can only obtained by diffraction methods, like laboratory XRD. Microscopic and micro spectrometric solutions work well in the cases were grains and textures are distinguished. But if we have greenstone tools, with macroscopically homogeneous structure, we barely can make difference between omphacitite, jadeitite and other green stone materials. In these cases, even local (SEM+EDS, Bendő et al. 2013) and more or less bulk (PGAA, Szakmány & Kasztovszky 2004)

chemical results may be hard to interpret. The aim of this study is to show how useful non-destructive XRD technique can be, applied to identify the rock type of rare and special stone tools, with easy and simple measurement and evaluation procedure.

Although application of Search/Match evaluation technique and the use of ICDD PDF databases is a "last century's" invention, the success of evaluation depends much on how the user can maximize data quality and searching criteria. Relative peak intensities of searched phases are as important in Search/Match evaluation, as peak positions. But preferred orientation usually produces anisotropic distortion of pattern, i.e. several peaks will be measured smaller, while others higher, than theoretical values. When working with powder pattern, these peaks can easily be identified, and intensity distortions either disregarded e.g. in multiple iteration Search/Match, or corrected by profile or pattern fitting. In both cases we can stop with evaluation without seeking partial solutions in vain. In the case of block samples, where orientation of crystals is determined by rock texture, we may observe one or just a few peaks of one phase. In these cases finding that phase is improbable, and correction of intensities may also become impossible. None the less, reduction of measurement and data evaluation time is crucial in the lack of stone tools research dedicated laboratories.

Materials and methods

A Bruker D8 Advance powder diffractometer was used, equipped with Cu-K$_\alpha$ source (40kV, 40mA), Göbel mirror and Våntec1 PSD detector, on a 250 mm radius goniometer, with 50 cm sample plane height (allowing large sample introduction). Since the Göbel mirror removes K$_\beta$ components of incident beam, filters or monochromators are not required. The Göbel mirror has < 0.25° primary equatorial divergence, thus an instrumental broadening of 0.145° (2θ) can be obtained, using 0.6 mm exit slit and 1 mm detector slit. Instrumental broadening as a measure of resolution means the minimal separation that can be observed between two neighbouring peaks on an ideally crystalline material. This resolution is maintained with Våntec1 on smooth and plain surfaces, slightly increasing at high angles, up to 0.150° (2θ). For non-destructive application, change in resolution and displacements were verified on the NIST1976 α-Al$_2$O$_3$ calibration standard. The instrument is equipped with primary beam shield and detector side beam stop (**Fig. 1.**).
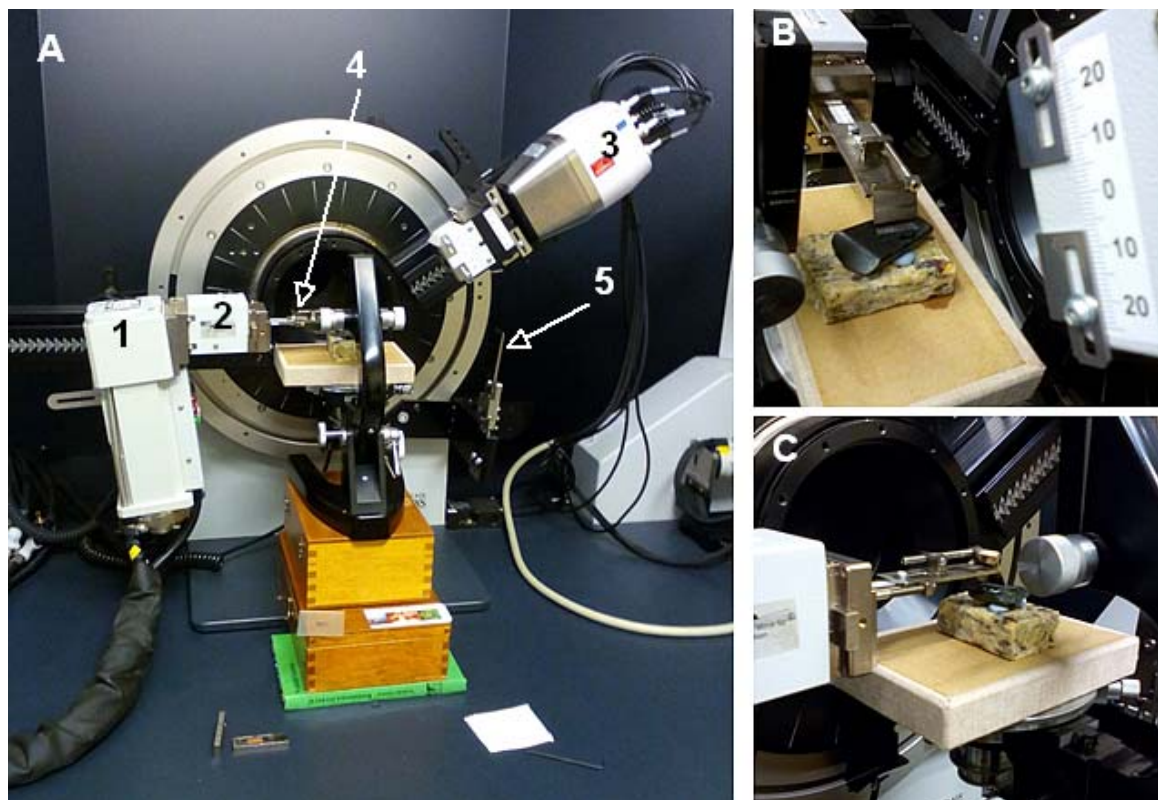
Fig. 1.: A: general view of the goniometer with sample mounted (1 – X-ray source, 2 – Göbel mirror, 3 – Vantec-1 PSD detector, 4 – incident beam cut-off knife edge, 5 – diffracted beam low angel cut-off shield) , B and C: view on the analyzed surface, marked with an Al-foil

1. ábra: A: a goniométer és beállított minta általános nézete (1 – sugárforrás, 2 – Göbel tükör, 3 – Vantec-1 PSD detektor, 4 – primer nyaláb szabályozó késlemez, 5 – diffraktált nyaláb alacsony szögű szabályozó késlemez).

Several green stone tools were measured, on one or more selected surface spots, to identify mineralogical constituents. Description of tools by the means of macroscopic features, their origin, and petrographic description is given in Péterdi et al. (2015) and Bendő et al. (2014). In lack of dedicated sample mounting system, the tools were mounted and aligned by the use of an optical microscope with dismounted stage with micro adjustment screws and rotate-tilt stage (**Fig. 1**.). The only required sample preparation was the cleaning with acetone of the selected plane and possibly smooth surfaces to be analysed. The selected surface was aligned in the sample plane in reference to the primary beam shield, since it is a fixed and highly centred part of the apparatus (**Fig. 1A and 1B**).

Evaluation of recorded patterns was done in Bruker Diffrac*Plus* EVA software, applying Search/Match algorithm for ICDD PDF2 (2005) database, on Fourier-polynomial smoothed (Wells & Brown 2009) and background removed curves. In some cases $K_{\alpha2}$ removal by Rachinger algorithm (Rachinger 1948, for an experimenttaly determined $K_{\alpha1}/K_{\alpha2}$ ratio) also proved useful, but it's not a

necessary data reduction step for successful evaluation. For a more detailed evaluation, Rietveld refinement can be applied, however in lack of knowledge on chemical composition this step may become unreliable.

Prior to presenting the obtained mineralogical data, a summary of instrumental alignment, set-up and testing on standards is presented. With the use of NIST 1976b standard the nature of peak shifting on specimen misalignment can be tested. The observed effect is known as parallax effect and it is arising from detector interface construction, and if it is not digitally corrected (Guinebretière 2013), it can be eliminated by goniometer and slit alignment. Its effect is eliminated in parallel beam geometry by minimizing detector window and slit opening. In our case it was found that a detector opening of 5° and a 0.1 mm beam exit slit gives reliable results (**Fig. 2.**). This allows us to run an 11 hours measurement in 10 minutes, without significant peak broadening arising from parallax effect. Depending on surface topography, the use of ± 0.01° to ± 0.06° 2θ-scale window could be required for Search/Match.
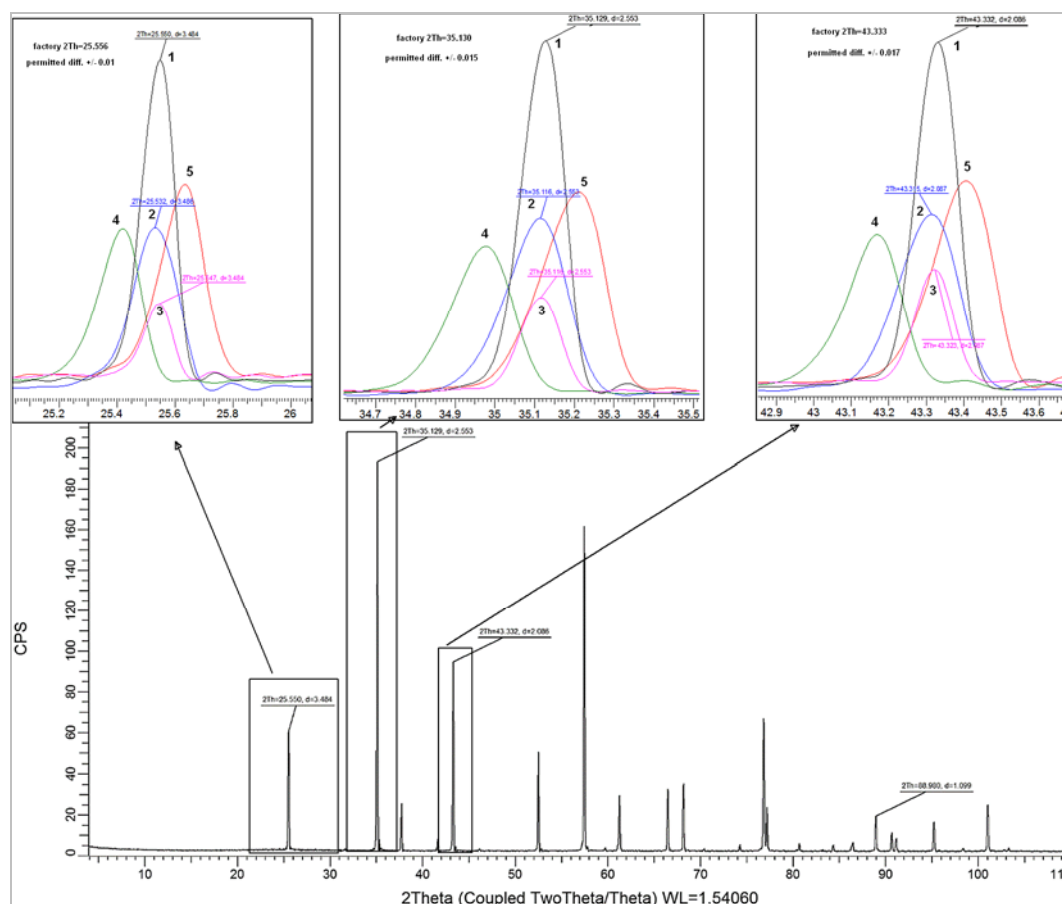
Fig. 2.: Patterns of NIST 1976b corundum calibration standard, 1 – pattern with powder stage and 0.6 mm exit slit with 1° Vantec window (15 minutes), 2 – pattern with stative used for ND-XRD, 0.6 mm exit slit with 1° Vantec window (5 minutes), 3 – pattern with stative used for ND-XRD, 0.1 mm exit slit with 5° Vantec window (5 minutes), 4,5 – patterns with ~0.5 mm misalignment (intensity differences are due to different recording times)

2. ábra: A NIST 1976b kalibrációs standardon mért görbék, 1 – gyári asztallal mért görbe, 0.6 mm kimeneti réssel és 1°Vantec ablakkal (15 perc), 2 – mikroszkópi állvánnyal mért görbe 0.6 mm kimeneti réssel és 1°Vantec ablakkal (5 perc), 3 - mikroszkópi állvánnyal mért görbe 0.1 mm kimeneti réssel és 5°Vantec ablakkal (5 perc), 4,5 - ~0.5 mm mintasík eltolódással mért görbe (az intenzitásbeli különbségek az eltérő mérési időkből adódnak

The mineralogical composition of samples is presented in tabulated form, with short mineral description, and also the evaluated patterns are shown, for graphical confirmation of results. The selecting of mineral species or groups is not arbitrary and is based on the matching precision of measured and theoretical peak positions on the first place. If the several first returned results do not fit the patterns, searching window ± limits must be widened. This evaluation process have helped us in the processing of several complex materials. We were able to differentiate omphacite and jadeite in greenstone tools, XRD result being in high agreement with chemical investigations (Szakmány et al. 2013). In the case of blueschist tools, we were able to match the glaucophane – ferroglaucophane series, confirmed by energy dispersive spectrometry too (Kereskényi et al. 2015).

After evaluating of XRD patterns, the investigated samples can be grouped in several major classes: (1) omphacite-jadeite eclogite type rocks with omphacitite and jadeitite compositions also, (2) amphibole dominated schists with actinolite schist and greenschist examples, (3) chlorite schists and (4) hornfels type contact metamorphic siliceous rock.

Results

(1) Omphacite-jadeite eclogite type

Before the presentation of results, a short summary on pyroxene crystal structures and XRD peaks is needed, in order to understand the evaluation process and results. Pyroxene structure is built up by silicate tetrahedra aligned in single chains along the "c" crystallographic axes bonded by oxygens, laterally – on "a" and "b" crystallographic axes – bonded by cations.
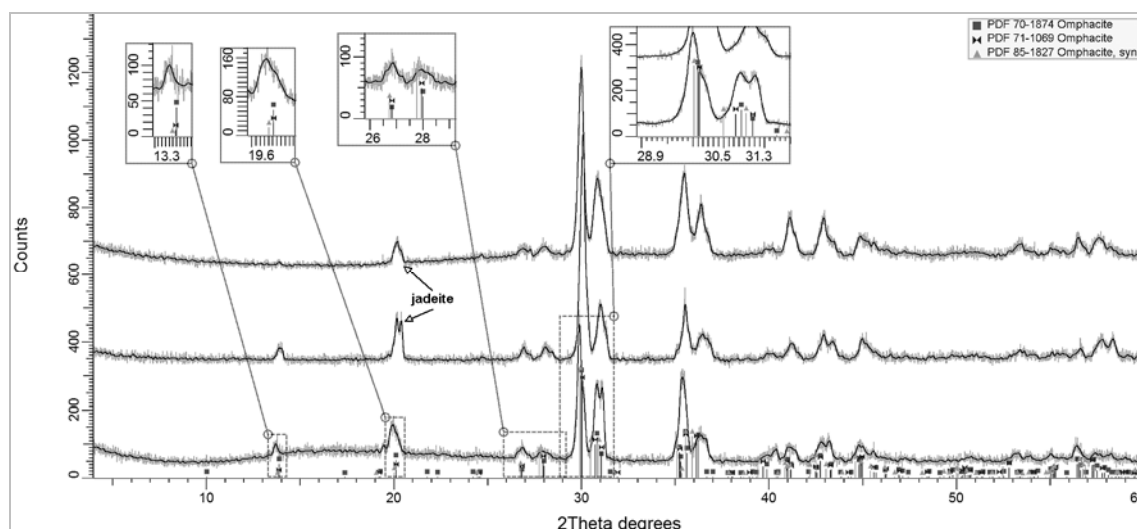
Table 1.: Theoretical peak position for several *C2/c* space group clinopyroxenes, showing differences in °(2θ) and ångströms (1/2I$_{FWHM}$ – half value of the instrumental peak full width at half maximum)

1. táblázat: Néhány *C2/c* tércsoportú klinopiroxén elméleti csúcspozíciói, a °(2θ) szög- és ångströmbeli különbségei (1/2I$_{FWHM}$ – a műszer félérték szélességének fele)

h	k	l	2θ				d(Å)		
			Diopside	Diopside +1/2I$_{FWHM}$	Omphacite	Jadeite	Diopside	Omphacite	Jadeite
1	1	0	13.70	13.77	14.16	14.28	6.458	6.196	6.248
0	2	0	19.94	20.01	20.54	20.41	4.450	4.347	4.320
1	-1	-1	20.18	20.25	20.71	20.73	4.397	4.281	4.285
0	2	1	26.66	26.74	27.27	27.46	3.340	3.245	3.268
2	2	0	27.60	27.68	28.55	28.79	3.229	3.098	3.124
2	-2	-1	29.92	29.99	30.85	30.63	2.984	2.917	2.896
1	-3	-1	35.04	35.12	35.51	35.56	2.559	2.523	2.526
2	0	-2	35.47	35.55	35.87	35.96	2.528	2.495	2.501
0	0	2	35.48	35.55	35.88	36.08	2.528	2.488	2.501
1	-1	-2	35.62	35.70	36.18	36.13	2.518	2.484	2.481
2	2	1	35.63	35.70	36.37	37.22	2.518	2.414	2.469
3	1	1	39.02	39.09	39.72	40.90	2.307	2.205	2.268
0	4	0	40.52	40.59	40.80	40.96	2.225	2.202	2.210
3	-1	-2	40.63	40.70	41.45	41.51	2.219	2.173	2.177
1	1	2	40.63	40.70	41.46	41.82	2.219	2.158	2.176
2	-2	-2	41.02	41.10	41.78	41.97	2.198	2.151	2.160
0	2	2	41.02	41.10	42.14	42.18	2.198	2.141	2.143
3	3	0	41.94	42.01	43.42	43.78	2.153	2.066	2.083
3	-3	-1	42.45	42.52	43.96	43.80	2.128	2.065	2.058
4	-2	-1	42.95	43.02	44.42	44.28	2.104	2.044	2.038
4	2	0	43.57	43.64	44.97	45.49	2.076	1.992	2.014
0	4	1	44.45	44.53	45.27	45.60	2.036	1.988	2.001
4	0	-2	45.04	45.11	45.97	46.13	2.011	1.966	1.972
2	0	2	45.04	45.11	46.16	46.75	2.011	1.941	1.965
2	4	0	45.06	45.13	46.80	46.99	2.010	1.932	1.939
1	-3	-2	46.13	46.21	47.08	47.16	1.966	1.925	1.929
2	-4	-1	46.62	46.69	48.34	48.22	1.947	1.886	1.881

| diopside, CaMgSi$_2$O$_6$ |
|---|
| a=9.746 Å, b=8.899 Å, c=5.251 Å, β=105.63° |
| omphacite (Ca,Na)(Mg,Fe^{2+},Al)Si$_2$O$_6$ |
| a=9.54-9.68 Å, b=8.57-8.90 Å, c=5.23-5.28 Å, β=105-108° |
| jadeite Na(Al,Fe^{3+})Si$_2$O$_6$ |
| a=9.418 Å, b=8.562 Å, c=5.219 Å, β=107.58° |

Table 2.: The position of most important peaks for omphacitic pyroxenes, plotted on **Fig. 3,** °(2θ) regions are: 1: 10-11°; 2: 13-14°; 3: 19-21°; 4: 26-27°; 5: 27-28°; 6: 29-32°; 7: 35-37°

2. táblázat: Omfacitos összetételű piroxének legfontosabb csúcsainak helye, (ld. a **3. ábrán**), a °(2θ) tartományok: 1: 10-11°; 2: 13-14°; 3: 19-21°; 4: 26-27°; 5: 27-28°; 6: 29-32°; 7: 35-37°

| °(2θ) region	PDF 70-1874 P2/n $a=9.622$ Å, $b=8.826$ Å, $c=5.279$ Å, $\beta=106.92°$ $Fe_{0.475}Al_{0.525}Ca_{0.492}Na_{0.508}(Si_2O_6)$				PDF 71-1069 C2/c $a=9.646$ Å, $b=8.824$ Å, $c=5.270$ Å, $\beta=106.598°$ $Na_{0.32}Ca_{0.59}Mg_{0.60}Fe_{0.25}Al_{0.24}(Si_2O_6)$				PDF 85-1827 C2/c $a=9.709$ Å, $b=8.874$ Å, $c=5.263$ Å, $\beta=106.34°$ $Mg_{0.89}Fe_{0.08}Al_{0.20}Cr_{0.04}Ti_{0.01}Ca_{0.76}Na_{0.10}(Si_{1.92}O_6)$			
	Angle	d Value	R.I. (%)	h,k,l	Angle	d Value	R.I. (%)	(h,k,l)	Angle	d Value	R.I. (%)	h,k,l
1	10.01	8.826	0.8	010								
2	13.88	6.371	13.5	110					13.77	6.426	0.40	110
3	19.26	4.603	1.5	200	19.18	4.622	0.30	200	19.036	4.658	0.40	200
3	20.10	4.413	17.3	020	20.11	4.412	9.00	-111	19.995	4.437	5.20	020
3	20.10	4.413	17.3	-111	20.11	4.412	9.00	020				
4	26.80	3.323	3.4	021	26.81	3.323	7.3	021	26.72	3.333	9.5	021
5	27.99	3.185	11.6	220	27.93	3.191	17.6	220	27.74	3.213	22.4	220
5	29.98	2.979	100	-221	30.00	2.976	100	-221	29.90	2.986	100	-221
6	30.82	2.898	38.4	310	30.70	2.909	34.9	310	30.47	2.931	31.8	310
6	31.04	2.879	18.7	-311	31.03	2.879	26.8	-311	30.91	2.89	32.3	-311
7	35.19	2.548	25.2	-131	35.22	2.546	25.6	-202	35.07	2.556	25.9	-131
7	35.19	2.548	25.2	-202	35.22	2.546	25.6	-131	35.31	2.539	4.4	-202
7	35.27	2.542	16.0	031								
7	35.52	2.525	40.5	002	35.52	2.525	40.3	-112	35.52	2.525	39.8	-112
7	35.52	2.525	40.5	-112	35.52	2.525	40.3	002	35.52	2.525	39.8	002
7	35.60	2.519	24.1	320					35.89	2.5	39.7	221
7	36.21	2.478	37.1	221	36.10	2.486	38.9	221	37.81	2.377	0.8	131
7	36.21	2.478	37.1	230					38.62	2.329	0.4	400
7									39.39	2.285	14.0	311

Fig. 3.: XRD patterns and matched phases PDF files (gray: original raw pattern, black: Fourier filtered and background modelled). Sample: 99.3.1863.

3. ábra: XRD görbék és a kiértékelés során kapott fázisok, PDF számmal (szürke: eredeti mért görbe, fekete: Fourier-polinommal simított és háttér illesztett). Minta: 99.3.1863
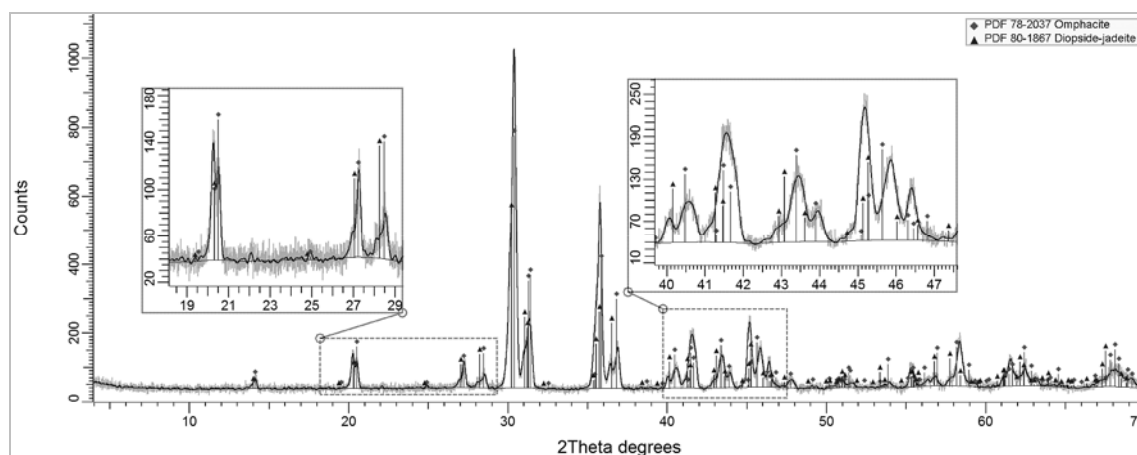
Fig. 4.: XRD patterns and matched phases PDF files (gray: original raw pattern, black: Fourier filtered and background modelled). Sample: N1/81-1938

4. ábra: XRD görbék és a kiértékelés során kapott fázisok, PDF számmal (szürke: eredeti mért görbe, fekete: Fourier-polinommal simított és háttér illesztett). Minta: N1/81-1938
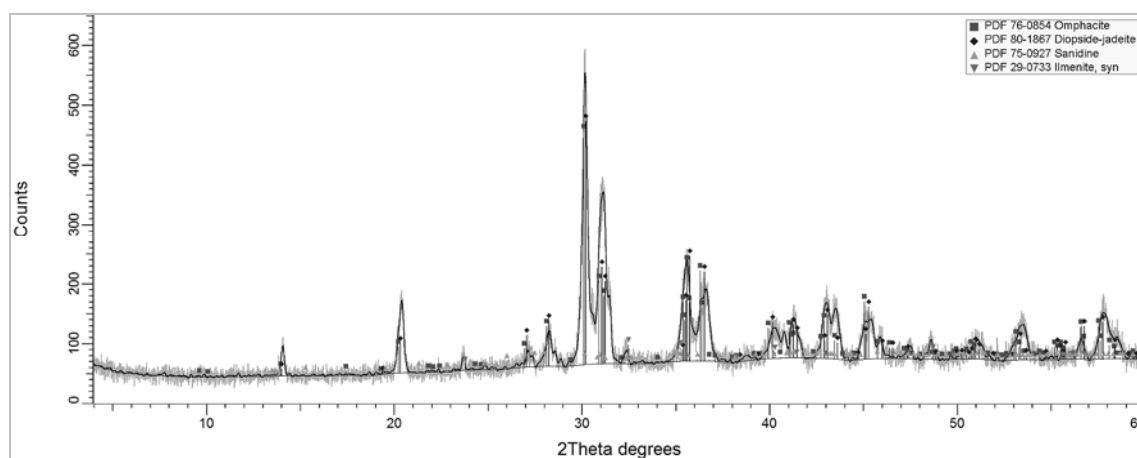
Fig. 5.: XRD patterns and matched phases PDF files (gray: original raw pattern, black: Fourier filtered and background modelled). Sample: N11/169-1938

5. ábra: XRD görbék és a kiértékelés során kapott fázisok, PDF számmal (szürke: eredeti mért görbe, fekete: Fourier-polinommal simított és háttér illesztett). Minta: N11/169-1938

As a consequence of cation arrangement along the chains, monoclinic and rhombic structural varieties are formed, known as clinopyroxenes and orthopyroxenes. The difference between the two types is readily deduced from diffraction data, but not for the identification of clinopyroxene species, their classification being done on chemical composition basis (Morimoto et al. 1988). The most clinopyroxenes have space group *C2/c*, and the differences in the end member phases XRD peaks positions are given by the distortions caused in the unit cell with the changing size and bond lengths of the cations. For instance, diopside and jadeite have similar structures (Prewitt & Burnham 1966), and if we calculate peak positions for their theoretical unit cells (Fehér 2009, a complete collection of valid mineral species description), we find some obvious, but very small differences in peak positions, more significant if we compare also with omphacite (**Table 1.**) Here, if we use the instrumental broadening (obtained on NIST 1976b corundum and verified with NIST 640a silicon) to extend the angular range for single peaks, we still may have enough differences in peak positions to delimit their maxima. Intensities for each individual peaks are influenced by chemical composition, but due to the large expected distortions arising from rock texture and surface morphology the relative intensities will become unreliable in mineral identification, thus the theoretical differences are not considered here. More important feature of these structures is their ability to form solid solutions, cation substitutions and cation ordering phenomena, which produce unit cell distortions (Nestola et al. 2007) and modulated structures expected on nanometric scale. These solid solution crystals are difficult to identify by XRD, but if there exists dominant end members, or dominant species in the samples, correct identification is possible. For instance, omphacite as a 1:1 solid solution of jadeite with diopside or hedenbergite will form with a different unit cell, *P2/n* (Nestola et al. 2007), which also will create additional differences in peak positions. The most important is the appearance of a peak at 10.22 ± 0.05° (2θ) (Cu-Kα source), but this peak can also be of very low intensity. Unfortunately, this nature of omphacitic solid solutions also gives room for a larger variability of peak position, in a -0.25° (2θ) with regard to the values in **Table 1**.

99.3.1863 "Gorzsa 11" tool

For 3 recorded patterns the Search/Match (± 0,05° window on 2θ-scale) returned omphacite as best match, and observed peak positions match the general clinopyroxene structure (*C2/c*, **Table 2.**). Shifting of peak positions (Nestola et al. 2007) due to cation substitution is considered, most of the omphacitic species have major peaks falling inside a ~0.10 ° (2θ) range, closed to the instrumental

broadening range, complicating the evaluation. Several of first matches of evaluation are plotted on **Fig. 3.** to demonstrate the effect of chemical composition on peak positions (Giustetto et al. 2008), according to database entries. Since jadeite or jadeite – diopside solution type phases were not returned, they are not plotted on **Fig. 3**. We observe the domination of *C2/c* structure, while diopside or other alkaline clinopyroxens are not found, and the found omphacite structures tend to a jadeite >> diopside solid solution. The SEM+EDS investigation (Bendő et al. 2014) of this tool proved the coexistence of omphacite, jadeite, ferrous jadeite and aegirine-augite.

N.1/81-1938 "JPM 1_81-1938" tool

The rock from which this tool was made is an almost pure omphacitite **(Fig. 4.)**, with some jadeite and Ca-bearing jadeite components, which is listed in the database as "jadeite – diopside" solution (**Table 3.**). The splitting of peaks at ~20° (2θ) angles is related to presence of both omphacite and C2/c phase(s) with different cations and narrow peaks indicate the well-developed crystalline nature of pyroxenes (crystallite sizes > 1μm). Some white spots were distinguished in its texture, but measurement trials resulted in patterns with very few peaks besides those of omphacite, thus phase identification was not possible, the patterns are not included here. The SEM+EDS investigation (Bendő et al. 2014) of this tool proved the coexistence of omphacite and jadeite, while the white spots were mainly epidote/zoisite + albite

N.11/169-1938 "JPM 1_169-1938" tool

Due to its homogeneous texture, with no visible spots or grains, one measurement was run on a larger surface. The pattern shows peaks of omphacite and jadeite-diopside as main phases, while sanidine (d$_{(130)}$=3.752 Å – 23.69 °2θ, d$_{(220)}$=3.273 Å – 27,215 °2θ) and ilmenite (d$_{(104)}$=2.754 Å – 32.48 °2θ) were identified based on several smaller peaks (**Fig. 5.**). The peaks with net height < 5 counts were not included in the evaluation, even if they belong to accessory phases, the uncertainty of identification is too high. The SEM+EDS investigation (Bendő et al. 2014) of this tool proved the coexistence of jadeite, ferrous jadeite and aegirine-augite. In this case, the observed omphacite peaks measured by XRD may be a consequence of aegirine-augite and ferrous jadeite presence, thus only jadeite is marked as certainly identified.

39/1903 "MNM 39-1903" tool

An omphacite – jadeite green stone (**Fig. 6.**), jadeite with larger crystallite sizes, thus better developed grains, according to minimal peak broadening.

Table 3.: Peak positions for omphacite (A) and jadeite-diopside solid solution phase (B), from ICDD PDF card

3. táblázat: Omfacit (A) és diopszid-jadeit (B) elegy fázis csúcspozíciói az ICDD PDF kártyák alapján

|	PDF 78-2037 (A) *C2/c* a=9.501 Å, b=8.654 Å, c=5.238 Å, β=107.23°				PDF 80-1867 (B) *C2/c* a=9.561 Å, b=8.730 Å, c=5.249 Å, β=10703°			
	Angle (°2θ)	d (Å)	R.I. (%)	h,k,l	Angle (°2θ)	d (Å)	R.I. (%)	h,k,l
1	14.13	6.263	4.6	1,1,0	14.02	6.314	2.7	1,1,0
2	20.31	4.369	7.8	-1,1,1	20.33	4.365	12.0	0,2,0
	20.51	4.327	16.4	0,2,0				
3	27.23	3.273	10.5	0,2,1	27.05	3.294	13.0	0,2,1
	28.48	3.131	13.7	2,2,0	28.25	3.157	18.6	2,2,0
4	30.40	2.938	100.0	-2,2,1	30.22	2.955	100.0	-2,2,1
	31.30	2.855	42.3	3,1,0	31.06	2.877	39.6	3,1,0
	31.41	2.846	44.8	-3,1,1	31.25	2.860	33.6	-3,1,1
5	35.87	2.501	50.4	0,0,2	35.54	2.524	24.9	-1,3,1
					35.75	2.510	42.9	0,0,2
					35.75	2.510	42.9	-1,1,2
	36.81	2.440	35.4	2,2,1	36.53	2.458	36.5	2,2,1
6	40.48	2.226	13.2	3,1,1	40.16	2.243	14.8	3,1,1
	41.49	2.175	13.9	1,1,2	41.27	2.186	13.6	1,1,2
					41.47	2.176	10.0	0,2,2
7	43.39	2.084	16.7	-3,3,1	43.08	2.098	17.9	-3,3,1
8	45.65	1.986	17.5	0,4,1	45.14	2.007	10.3	-4,0,2
					45.27	2.001	21.3	0,4,1
9	56.96	1.615	13.0	-2,2,3	56.79	1.620	13.6	-2,2,3
					57.76	1.595	15.0	-5,3,1
					57.76	1.595	15.0	1,5,1
	58.19	1.584	15.2	1,5,1				
	58.19	1.584	15.2	-5,3,1				
10	62.44	1.486	13.0	-5,3,2	62.15	1.492	13.3	-1,3,3
	62.44	1.486	13.0	-1,3,3	62.15	1.492	13.3	-5,3,2
11	67.83	1.381	10.6	-3,5,2	67.53	1.386	19.9	5,3,1
	68.14	1.375	14.7	2,6,0	67.53	1.386	19.9	2,6,0
	68.14	1.375	14.7	5,3,1				
A: $Ca_{0.29}Na_{0.6}Al_{0.76}Mg_{0.21}Fe_{0.08}(Al_{0.01}Si_{1.99}O_6)$								
B: $(Ca_{0.47}Na_{0.41}Fe_{0.04}Mg_{0.02})(Mg_{0.44}Fe_{0.03}Ti_{0.01}Al_{0.52})(Si_2O_6)$								
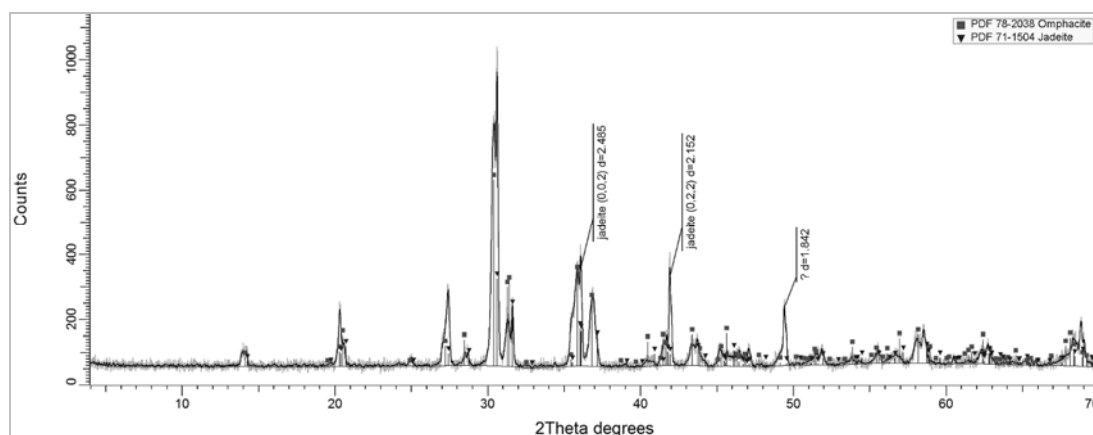
Fig. 6.: XRD patterns and matched phases PDF files (gray: original raw pattern, black: Fourier filtered and background modelled). Sample: 39/1903

6. ábra: XRD görbék és a kiértékelés során kapott fázisok, PDF számmal (szürke: eredeti mért görbe, fekete: Fourier-polinommal simított és háttér illesztett). Minta: 39/1903
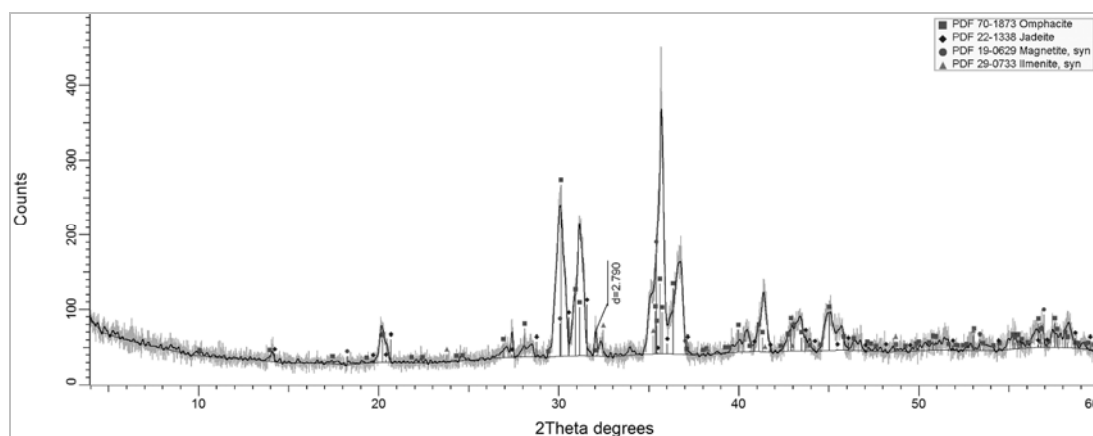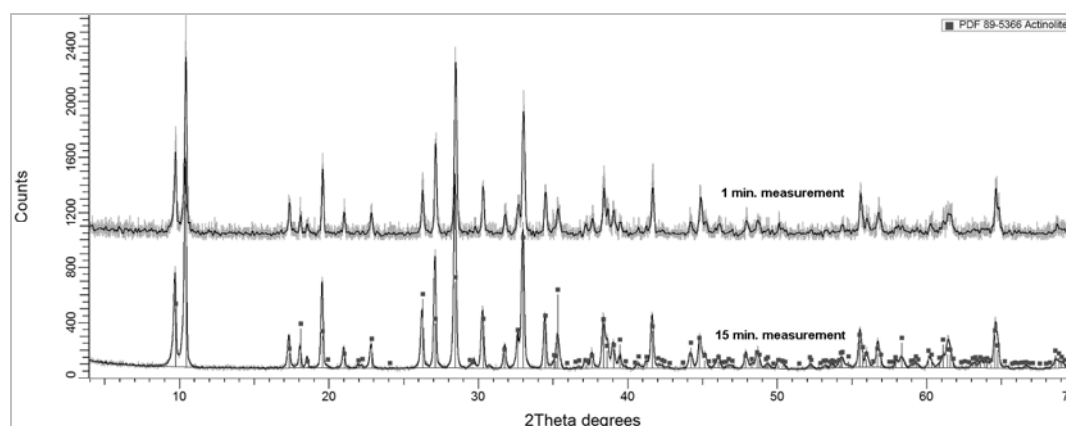

Fig. 7.: XRD patterns and matched phases PDF files (gray: original raw pattern, black: Fourier filtered and background modelled). Sample: Olad-329

7. ábra: XRD görbék és a kiértékelés során kapott fázisok, PDF számmal (szürke: eredeti mért görbe, fekete: Fourier-polinommal simított és háttér illesztett). Minta: Olad-329
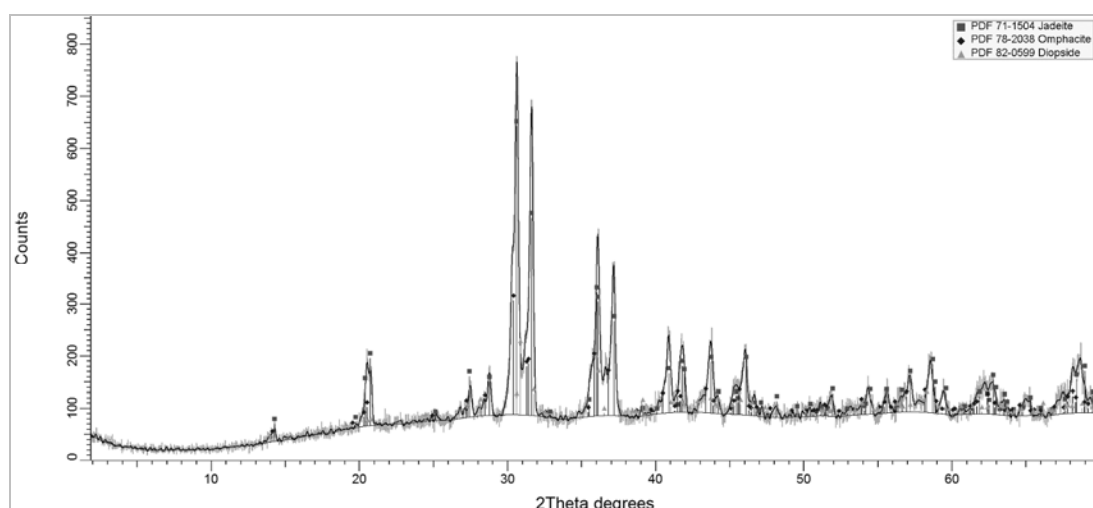
Fig. 8.: XRD patterns and matched phases PDF files (gray: original raw pattern, black: Fourier filtered and background modelled). Sample: 81/W2.5

8. ábra: XRD görbék és a kiértékelés során kapott fázisok, PDF számmal (szürke: eredeti mért görbe, fekete: Fourier-polinommal simított és háttér illesztett). Minta: 81/W2.5

Table 4.: Main theoretical peak positions of several clinoamphiboles, calculated according to their unit cell in Fehér (2009), calculated for Cu-Kα radiation

4. táblázat: Néhány klinoamfibol elméleti csúcspozíciói, Fehér (2009) által megadott elemi cellából Cu-Kα sugárzásra számolva

| h k l	1 (°2θ)	2 (°2θ)	3 (°2θ)	4 (°2θ)	5 (°2θ)
0 2 0	9.71	9.79	9.79	9.72	9.78
1 1 0	10.44	10.48	10.46	10.39	10.34
		17.34	17.28	17.23	17.13
1 3 0	17.29	17.42	17.39	17.27	17.31
1 -1 -1	18.08	18.14	18.00	18.01	18.03
2 0 0	18.53	18.59	18.54	18.42	18.27
0 4 0	19.49	19.66	19.65	19.50	19.63
0 2 1	19.84	19.95	19.90	19.82	19.76
2 2 0	20.96	21.06	21.00	20.86	20.76
2 0 -1		21.99	21.78	21.80	21.83
1 1 1	22.15	22.27	22.26	22.12	21.89
1 -3 -1	22.78	22.91	22.78	22.73	22.80
2 -2 -1	24.05	24.13	23.93	23.91	23.97
0 4 1	26.15	26.33	26.28	26.14	26.00
1 3 1	26.16	26.33	26.32	26.14	26.17
1 5 0	26.17	26.38	26.35	26.16	26.28
2 4 0	27.02	27.19	27.14	26.95	26.94
3 1 0	28.38	28.49	28.40	28.22	28.00
2 0 1		28.66	28.67	28.44	28.09
3 -1 -1	29.38	29.45	29.20	29.17	29.17
0 6 0	29.42	29.67	29.49	29.41	29.52
2 -4 -1	29.52	29.68	29.66	29.44	29.63
1 -5 -1	30.16	30.35	30.26	30.12	29.81
2 2 1	30.19	30.36	30.37	30.12	30.26
3 3 0	31.66	31.81	31.73	31.52	31.36
3 -3 -1	32.57	32.69	32.45	32.38	32.42
1 5 1	32.84	33.07	33.06	32.82	32.78
1 -1 -2	34.14	34.27	34.05	34.04	33.97
0 6 1	34.31	34.57	34.53	34.31	34.42
2 4 1	34.78	35.00	34.97	34.73	34.50
0 0 2	34.93	35.09	35.00	34.87	34.66
2 6 0	35.00	35.25		34.95	35.03
2 0 -2	35.23	35.34		35.07	35.10
1 7 0	35.76	36.06		35.76	35.96
1. Actinolite $Ca_2(Mg,Fe^{2+})_5Si_8O_{22}(OH)_2$					
2. Tremolite $[]Ca_2Mg_5Si_8O_{22}(OH)_2$ ([]=vacancy)					
3. Potasscipargasite $(Na,K)Ca_2(Mg,Fe^{2+})_5Si_8O_{22}(OH,F)_2$					
4. Ferrohornbelnde $[]Ca_2[Fe^{2+}_4(Al,Fe^{3+})]Si_7AlO_{22}(OH)_2$					
5. Arfvedsonite $NaNa_2(Fe^{2+}_4Fe^{3+})Si_8O_{22}(OH)_2$					

Fig. 9.: XRD patterns and matched phases PDF files (gray: original raw pattern, black: Fourier filtered and background modelled). Sample: KGY-1

9. ábra: XRD görbék és a kiértékelés során kapott fázisok, PDF számmal (szürke: eredeti mért görbe, fekete: Fourier-polinommal simított és háttér illesztett). Minta: KGY-1
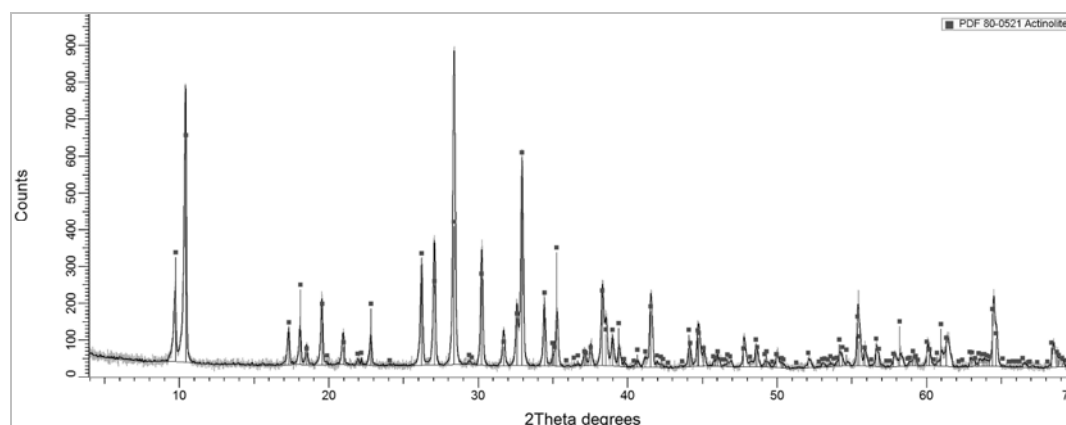
Fig. 10.: XRD patterns and matched phases PDF files (gray: original raw pattern, black: Fourier filtered and background modelled). Sample: SM-KE64

10. ábra: XRD görbék és a kiértékelés során kapott fázisok, PDF számmal (szürke: eredeti mért görbe, fekete: Fourier-polinommal simított és háttér illesztett). Minta: SM-KE64
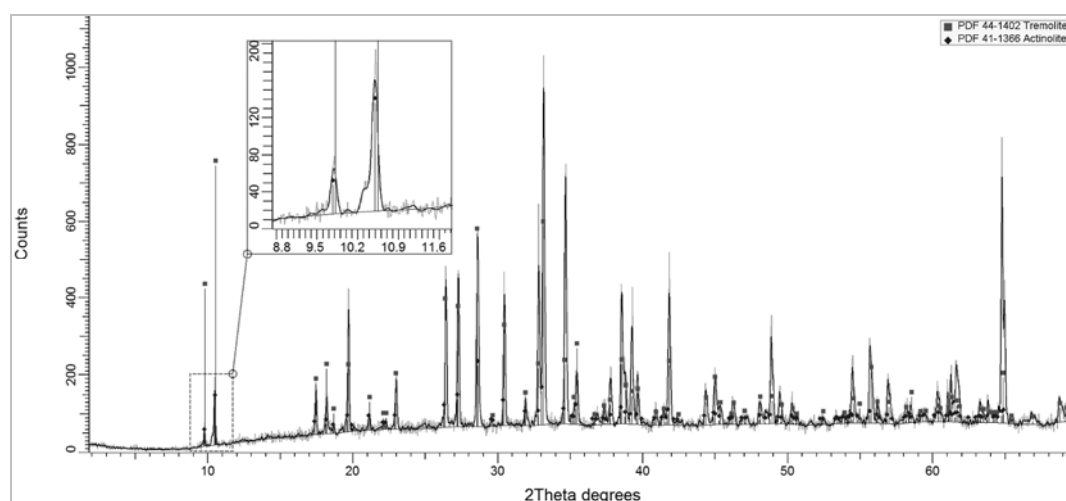
Fig. 11.: XRD patterns and matched phases PDF files (gray: original raw pattern, black: Fourier filtered and background modelled). Sample: WE 18 3.3

11. ábra: XRD görbék és a kiértékelés során kapott fázisok, PDF számmal (szürke: eredeti mért görbe, fekete: Fourier-polinommal simított és háttér illesztett). Minta: WE 18 3.3

Also the preferred orientation of (*002*) and (*022*) peaks indicates an oriented texture in the measured surface, with possibly platy crystallites of jadeite. The SEM+EDS investigation (Bendő et al. 2014) of this tool proved the coexistence of jadeite and ferrous jadeite.

Olad-329 "SM 329" tool

This tool is also omphacite – jadeite rock, with some minor unsolved peaks, which may belong to accessory minerals (**Fig. 7.**). In contrast with previous omphacite – jadeite samples, the presence of magnetite ($d_{(311)}$=3.531 Å – 35.43 °2θ) is highly possible in this sample. The SEM+EDS investigation (Bendő et al. 2014) of this tool proved the coexistence of omphacite and jadeite.

81/W2.5 "WE 81_W2-5" tool

The main phase returned by Search/Match is jadeite, with omphacite and uncertain diopside - according to (*110*) peak position - (**Fig. 8.**), a ± 0.05° (2θ) window on 2θ-scale had to be applied. The SEM+EDS investigation (Bendő et al. 2014) of this tool proved the dominance of jadeite with minor omphacite.

(2) Amphibole dominated schists, amphibolites

A short summary of amphibole structures is needed here also, since the amphiboles, structurally related to pyroxenes, are also difficult to be identified on a species level by XRD. The $[SiO_4]^{2-}$ anions form double chains, bridged by cations, and additional anions, mainly OH^- but also F^- (and more or less Cl) are incorporated to obtain structure neutrality. Cation ordering and distribution also creates the clino- and ortho series, but substitution and solid solution forming possibilities are greater than for pyroxenes. The classification is based on chemical compositional fields (Hawthorne et al. 2012), with multiple solid solution series and joints. Position of major peaks, calculated based on the unit cell given in Fehér (2009), for common clinoamphiboles are listed in **Table 4.**

"KGY 1" tool

This is a nephrite (=ferroactinolite – tremolite made fine grained or fibrous amphibolite, Zhou & Feng 2010) tool, with well-polished smooth surfaces, characteristic well visible fibrous texture. The first matching result was actinolite, with all the peak positions in >95% accordance of measured pattern (**Fig. 9.**). Although clinoamphibole species are more complicated to identify by Search/Match, than clinopyroxenes, in this case the match was acceptable. Even the oriented, long fibrous texture of the material did not produce complex preferred orientation effects. Pattern with good statistics was obtained with measurement time as low as 1 minute (**Fig. 9.**).

"SM KE64" tool

This tool is made up by amphibole, best match is actinolite (**Fig. 10.**) with minor preferred orientation and good agreement between theoretical and measured peak positions.

"WE 18_3-3" tool

In this tool, clinoamphibole presence is exclusive, as rock forming phase, but the Search/Match returned acceptable hits by applying the ± 0.1° (2θ) window on 2θ-scale. The best match was tremolite, with actinolite (**Fig. 11.**) retrieved in the second Search/Match iteration. Peak intensities are severely distorted due to surface morphology effects, the lack of plane surfaces resulted in shielding effect, either at low or high angles. We opted to record the higher angle region, most of the amphibole peaks being observed there.

"WE 67_W2-6" tool

The material of tool is amphibole dominant, mainly pargasite, but the presence of actinolite and tremolite is also likely. In contrast with the other amphibole rocks, this contains also sanidine and magnetite as rock forming phases, possibly with albite and anatase as accessory phases (**Fig. 12.**). Several major peaks and more small peaks remain unsolved, as these probably belong to the amphibole structure(s). Speculating on accessory phases would be inadequate, since peak positions may also be shifted by stress and strain, which is likely to affect minerals of metamorphic rocks.

"WE 81_W1-58" tool

This tool is dominantly made up by alkaline amphiboles, mainly by gedrite (**Fig. 13.**). Several more phases were observed as rock forming minerals, such as anorthite, pyrope garnet and ilmenite with magnesium substitution.

(3) Chlorite schists

The mineralogy and XRD identification of chlorite species is as complex as of amphiboles and pyroxenes. However, given the phyllosilicate layered type structure, cation distribution and substitution has some characteristic effect on (*00l*) type peaks position, although differences can properly be observed on the (*0l0*) peaks and their relative intensities (**Table 5.**). Even if polytypes cannot be identified with these peaks, the chlorite structure can be recognised.

"SM 9-14-10_1" tool

The material of this tool is hardly classified as a specific rock type, since it is made up by clinochlore alone, with some trace presence of biotite (**Fig. 14.**).
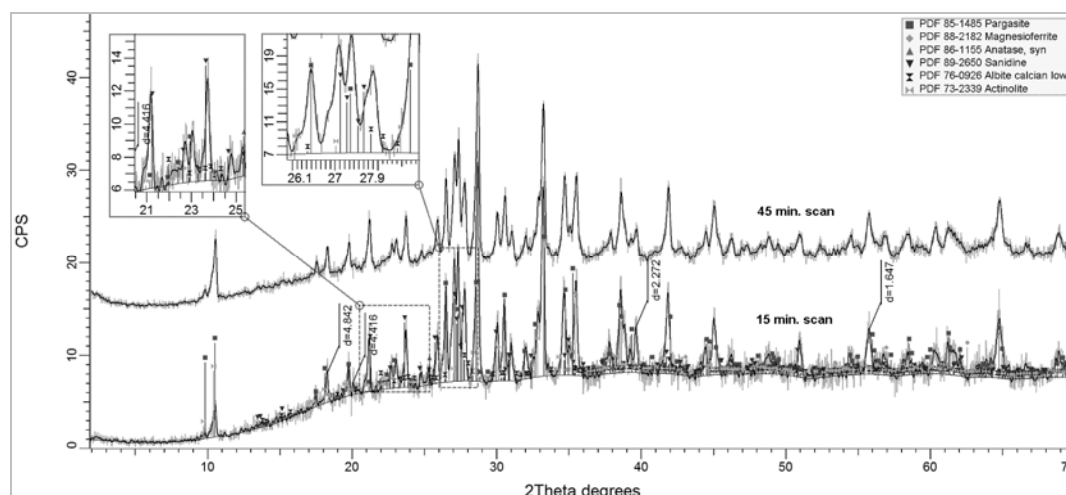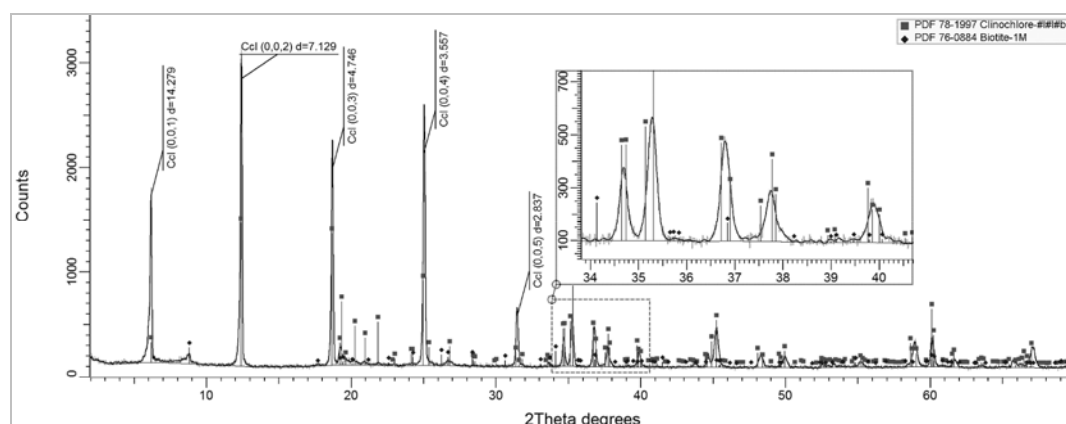
Fig. 12.: XRD patterns and matched phases PDF files (gray: original raw pattern, black: Fourier filtered and background modelled). Sample: 67/W2.6

12. ábra: XRD görbék és a kiértékelés során kapott fázisok, PDF számmal (szürke: eredeti mért görbe, fekete: Fourier-polinommal simított és háttér illesztett). Minta: 67/W2.6
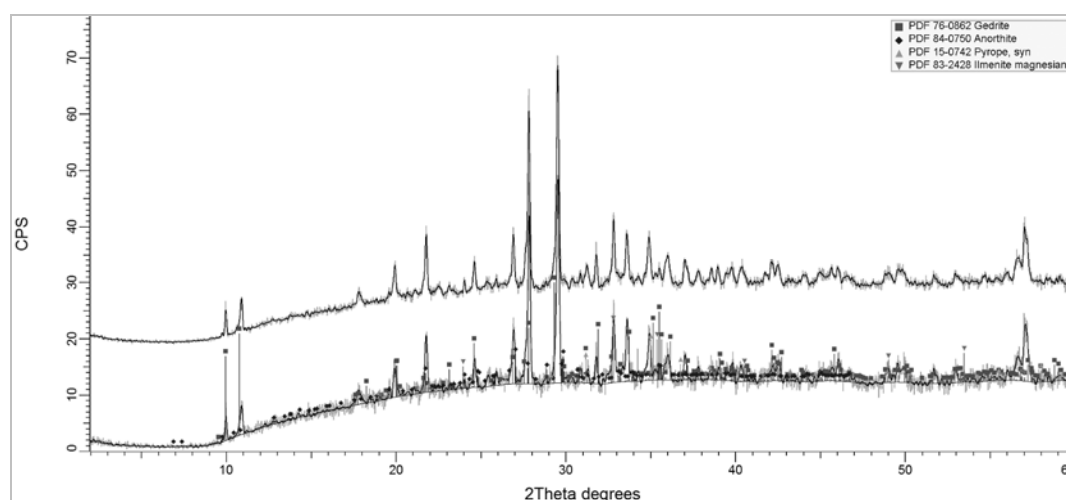
Fig. 13.: XRD patterns and matched phases PDF files (gray: original raw pattern, black: Fourier filtered and background modelled). Sample: 81/W1.58

13. ábra: XRD görbék és a kiértékelés során kapott fázisok, PDF számmal (szürke: eredeti mért görbe, fekete: Fourier-polinommal simított és háttér illesztett). Minta: 81/W1.58

Fig. 14.: XRD patterns and matched phases PDF files (gray: original raw pattern, black: Fourier filtered and background modelled). Sample: SM 9-14-10

14. ábra: XRD görbék és a kiértékelés során kapott fázisok, PDF számmal (szürke: eredeti mért görbe, fekete: Fourier-polinommal simított és háttér illesztett). Minta: SM 9-14-10

Table 5.: Variation of (00l) peaks position in clinochlore polytypes with chemical composition

**5. táblázat:** Klinoklór politípek (*00l*) típusú csúcsainak helye, kémiai összetételtől függően

(h,k,l)	1 Clinochlore-1MIIb PDF 46-1322	2 Clinochlore-1MIIb ferroan PDF 29-0701	3 Clinochlore 2a* PDF 73-2376	4 Clinochlore 1Mia PDF 89-2972
(0,0,1)	14.200	14.100	14.368	14.165
(0,0,2)	7.100	7.070	7.184	7.082
(0,0,3)	4.750	4.710	4.789	4.721
(0,0,4)	3.554	3.540	3.592	3.541
(0,0,5)	2.840	2.828	2.874	2.833
1 $Mg_5Al(Si,Al)_4O_{10}(OH)_8$				
2 $(Mg,Fe)_6(Si,Al)_4O_{10}(OH)_8$				
3 $Mg_6Si_4O_{10}(OH)_8$				
4 $Mg_{2.5}Fe_{1.65}Al_{1.5}Si_{2.2}Al_{1.8}O_{10}(OH)_8$				

Even if the (005) and some other peaks of the best matching structure are displaced, the measured phase corresponds to a magnesian clinochlore (Zheng & Bailey 1989). The strong preferred orientation of (0,0,l) type peaks is due to the oriented texture of the rock material, signalling a dinamometamorphic origin. Also, given the coincidence of chlorite lamellae parallelisms to the plate tool surface, indicates that the objects were fabricated from cleaved blocks of schist. The presence of platy, greenish matrix (**Fig. 15a**) and green transparent grains were observed by stereomicroscopy (**Fig. 15b**). The black metallic fragments could be iron oxide (e.g. magnetite) but biotite is also possible, while the orange grainy masses are Fe oxy-hydroxide alterations.

**(4) Hornfels type contact metamorphic siliceous rock**

"HOM 53-66-10" tool

The tool has a texture with no visible patches, homogeneously green coloured, one pattern was recorded. The Search/Match with ± 0,05° window on 2θ-scale returned quartz and plagioclase varieties as highly matching phases.
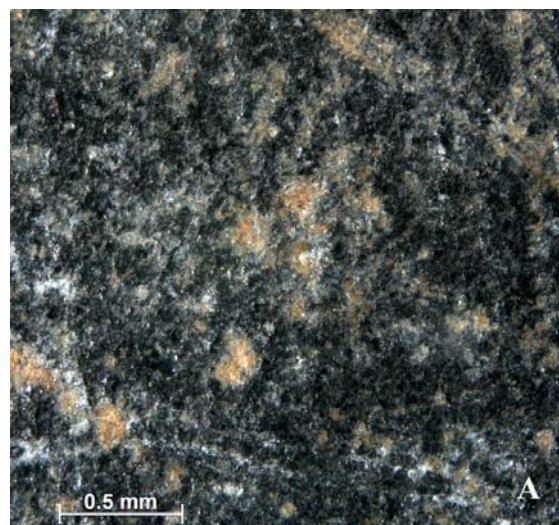
Fig. 15.: Stereomicroscopic images of chloritic rock (sample SM 9-14-10), a – texture in general, b – chlorite grains

15. ábra: Sztereomikroszkópos felvétel a kloritpaláról (SM 9-14-10 jelű minta), a – a kőzet szövete, b – klorit szemcse

On a second iteration, run for peaks other than quartz (SiO_2, trigonal) and calcian albite [$(Na_{0.9},Ca_{0.1})AlSi_3O_8$], ferroan clinochlore 1MIIb [$(Mg,Fe)_6(Si,Al)_4O_{10}(OH)_8$], epidote [$Ca_2Al_{2.4}Fe_{0.6}(SiO_4)_3(OH)$], magnesian ilmenite ($Mg_{0.208}Fe_{0.955}Ti_{0.833}O_3$) and muscovite [$(KAl_2(AlSi_3O_{10})(OH)_2$]was retrieved – chemical compositions according to ICDD PDF files. As it is marked in **Fig. 16.** some K-feldspar would be expected, but since no clearly distinguished peaks are observed, it was omitted from the results.
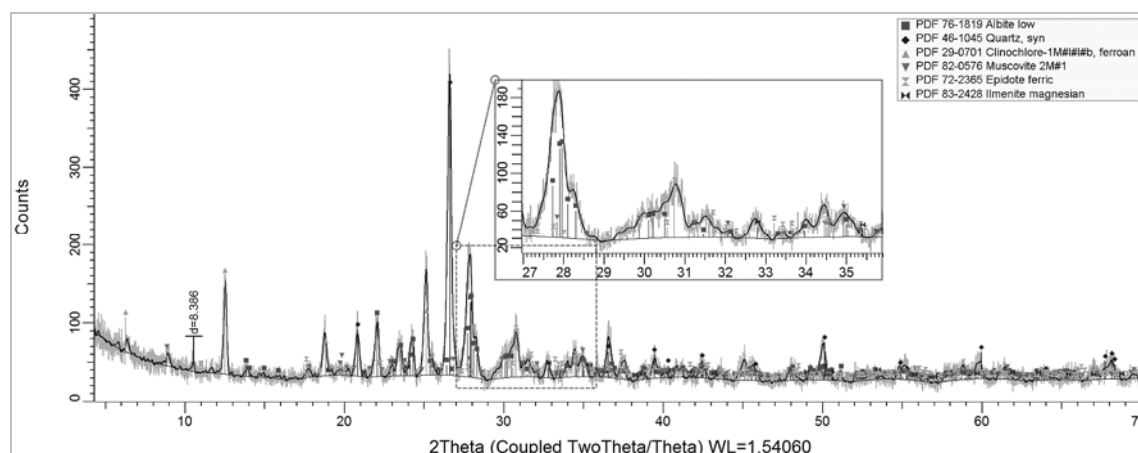
Fig. 16.: XRD patterns and matched phases PDF files (gray: original raw pattern, black: Fourier filtered and background modelled). Sample: HOM 53.66.10

16. ábra: XRD görbék és a kiértékelés során kapott fázisok, PDF számmal (szürke: eredeti mért görbe, fekete: Fourier-polinommal simított és háttér illesztett). Minta: HOM 53.66.10

Discussion

Peak positions were accurate enough in all measurements to conclude in successful Search/Match evaluation of patterns. As a routinely used evaluation process in our lab, it's useful to run the Search/Match in several iterations, creating "diff patterns" as secondary raw data, from the unidentified peaks. This way, in each step we have a set of peaks which defines a new intensity – position data range, maximizing exact phase matching even at accessory minerals level. However, when only a few peaks are left, usually no acceptable hits are returned by the algorithm, thus a limit of the method is met. A matched phase may be accepted as valid if all theoretical peaks appear in the measured data, or we can deduce the cause or peak shifts (e.g. chemical substitution, solid solution series or strained structure). If most of the peaks are overlapping with those of major phases, and intensity distributions cannot be solved, then again we cannot accept that phase as valid without validating with other methods.

The most attention demanding task is the alignment of specimen surface, which can be done with the given goniometer equipment, without the exclusive need of precision centring sample stage. Even if needed, currently available precision sample stage compatible with this type of equipment don't met the requirements, being built without tilting and oblique sample rotating possibilities. Without these options specimen surfaces cannot be optimally adjusted to the goniometer.

Measurement times down to 1 minute already enabled the correct identification of rock forming minerals at least on group level. On well-polished, plane surfaces counting time can be reduced, since most of the diffracted intensity reaches the detector, and is integrated in registered pattern. However, if specimen surface is scarred and bent or uneven, the beam optics setting will prevent X-ray photons diffracted at larger than $\pm 0.06°$ (2θ) diffraction angle difference to reach the detector. This reduces recorded intensity and low counting statistics results in useless pattern. On the basis of our observations, the choice on counting time will be easily determined according to macro geometric properties of tools.

Comparing the patterns and selected peaks of omphacite – jadeite samples, we can observe several characteristic differences. Peak positions, broadening and degree of overlapping may be used to differentiate between samples. According to measured peak maxima and overlapping, we observe ompachite with variable Ca-Al content and also jadeite with variable Fe content, even in transition to diopside (**Table 6.**). Changes in peak intensity are not suitable to use, due to complex preferred orientations, improbable to determine and model correctly.

Discrimination of amphibole species on crystal structure criteria is generally not accepted in mineralogist communities, since influence of cations on diffraction patterns is minimal. However, a sample dominated by one species with few cation substitutions measured on a diffractometer with good alignment and set-up, could result in identification of that species. Colour, on the other hand, is not plausible to be used as identification criteria of amphiboles, but still it will give information on the Fe^{2+} content of the species.

Table 6.: Omphacite-jadeite eclogite type pyroxenite tools composition
6. táblázat: Omfacit-jadeit eklogit típusú piroxenit eszközök összetétele

xxx=dominant xx=secondary x=accessory	omphacite	jadeite-diopside	jadeite	diopside	other
99.3.1863 "Gorzsa 11"	xxx	?			
N.1/81-1938 "JPM 1_81-1938"	xxx	xx			
N.11/169-1938 "JPM 1_169-1938"	xx	xx	?		sanidine, ilmenite
39/1903 "MNM 39-1903"	xxx		xxx		
Olad-329 "SM 329"	xxx		x		magnetite, ilmenite
81/W2.5 "WE 81_W2-5"	x		xxx	x	

Table 7.: Amphibole schist, amphibolite tools composition
7. táblázat: Amfibol palák, amfibolit eszközök összetétele

	Actinolite	Tremolite	Pargasite	Gedrite	other
KGY 1	xxx				
SM KE64	xxx				
WE 18_3-3	xx	xxx			
WE 67_W2-6	xx		xx		magnetite, anatase, sanidine, albite
WE 81_W1-58				xxx	anorthite, pyrope, ilmenite

That is, in the specimen where we identified tremolite and gedrite, the tool was made up by white to grey fibrous material. Strongly oriented textures are expected to be characteristic, for high pressure samples mainly. Accordingly, if preferred orientation is not observed, it may suggest that the specimen is not linked to high pressure metamorphism. This could be of interest in special in the cases of nephrite type tools, given their disputed petrogenesis (Liu et at. 2011) between serpentinite related metasomatic, dolomite related contact metamorphic or regional metamorphic origin. The later one could be separated from metasomatism related materials based on dominant preferred orientation of crystallites. Summary of investigated specimens is given in **Table 7**.

Conclusions

The results of our experiments can be summarized in several important conclusions. First of all, we managed to use a unique combination of X-ray optics and detectors for non-destructive investigation of larger than usual samples, without conventional sample stages. The results of Search/Match evaluation proved to be in accordance with chemical investigations. Given the short recording times, and minimal number of measurements, this positive feedback is significant. Of course, increasing recording times and measurement number will create a more useful data package, with possible application in the petrogenetical characterization of greenstone materials. But the rapid screening is essential and cannot be skipped in order to find the best specimens for detailed investigation.

Selection of rock materials improbable to differentiate by other methods is straightforward. Chlorite and chloritic schists, amphibole bearing schists or amphibolites and pyroxenites, even with mineralogic subtypes, are easily recognized.

According to observations of actinolite amphibolites, even semiquantitative textural information could be extracted, e.g. for the degree of amphibole orientations and crystallite shapes. This information could be useful to determine amphibolite origin.

Acknowledgments

References

BENDŐ, Zs., OLÁH, I., PÉTERDI, B., SZAKMÁNY, Gy. & HORVÁTH, E. (2013): Non-destructive SEM-EDX analytical method for polished stone tools and gems: opportunities and limitations. *Archeometriai Műhely* **10/1** 51–66.

BENDŐ, Zs., SZAKMÁNY, Gy., KASZTOV-SZKY, Zs., MARÓTI, B., SZILÁGYI, Sz., SZILÁGYI, V. & T. BIRÓ, K. (2014): Results of non-destructive SEM-EDX and PGAA analyses of jade and eclogite polished stone tools in Hungary. *Archeometriai Műhely* **11/4** 187–206.

BRENTANO, J.C.M. (1946): Parafocusing properties of microcrystalline powder layers in X-ray diffraction applied to the design of X-ray goniometers. *Journal of Applied Physics* **17** 420–434.

CHIARI, G., COMPAGNONIA, R. & GIUSTETTO, R. (1996): Use of non destructive X-Ray Diffraction Analyses. *Trace, on-line rock art bulletine* **5** http://www.rupestre.net/tracce/?p=1076

DESLATES, R.D., STAUDENMANN, J.L:, HUDSON, L.T., HEINS, A. & CLINE, J.P. (1997): Parallel beam powder diffractometry using a laboratory X-Ray source. International Centre for Diffraction Data, *Advances in X-ray Analysis* **40** 225–236.

DURAN, A., HERRERA, L.K., JIMENEZ DE HARO, M.C.,. JUSTO, A, PEREZ-RODRIGUEZ, J.L. (2008): Non-destructive analysis of cultural heritage artefacts from Andalusia, Spain, by X-ray diffraction with Goebel mirrors. *Talanta* **76** 183–188.

FEHÉR B. (2009): *Ásványkalauz*. Magyar Minerofil Társaság, Miskolc, 624 p.

GAN, F.X., CAO, J.Y., CHENG, H.S., GU, D.H., RUI, G.Y., FANG, X.M., DONG, J.Q. & ZHAO H.X. (2010): The non-destructive analysis of ancient jade artifacts unearthed from the Liangzhu sites at Yuhang, Zhejiang. Science China, *Technological Sciences*, **53/12** 3404–3419.

GIUSTETTO, R., CHIARI, G. & COMPAGNONIA, R. (2008): An easy non-invasive X-ray diffraction method to determine the composition of Na-pyroxenes from high-density `greenstone' implements. *Acta Crytsallographica Section A*, **64/1** 161–168.

GUINEBRETIÈRE, R. (2013): *X-Ray Diffraction by Polycrystalline Materials*. John Wiley and Sons, New York , 361 p.

HOLZ, T., DIETSCH, R., MAI, H. & BRÜGEMANN, L. (2000): Application of Ni/C-göbel mirrors as parallel beam X-ray optics for Cu-Ka and Mo-Ka radiation. International Centre for Diffraction Data, *Advances in X-ray Analysis* **43** 212–217.

HAWTHORNE, F.C., OBERTI, R., HARLOW, G.E., MARESCH, V.W., MARTIN, R.F., SCHUMACHER, J.C., & WELCH, M.D. (2012): Nomenclature of the amphibole supergroup, IMA Report. *American Mineralogist* **97** 2031–2048.

KERESKÉNYI, E., KRISTÁLY, F., FEHÉR B. & RÓZSA, P. (2015): Fisrt results on the archaeometric reserach of neolithic polished stone tools of the Herman Ottó Museum. Annual Meeting of Petrologists, Conference Proccedings *in press (in Hungarian)*

KOCKS, U.F., TOMÉ, C.N. & WENK, H.R. (2000): *Texture and anisotropy: preferred orientations in polycrystals and their effect on materials properties.* Cambridge University Press, 676 p.

KRISTÁLY, F. & KOVÁCS, P. (2011): Archaeological and preliminary archaeometrical investigations on the ceramic findings from nr. 3 site of the celtic cemetery at Hejőpapi excavated in 2008. *Archeometriai Műhely* **8/3** 251–268.

LIU, Y., DENG, J. SHI, G., YUI, T.-F., ZHANG, G., ABUDUWAYITI, E., YANG, L. & SUN, X. (2011): Geochemistry and petrology of nephrite from Alamas, Xinjiang, NW China. *Journal of Asian Earth Sciences* **42** 440–451.

MORIMOTO, N., FABRIES, J., FERGUSON, A.K., GINZBURG, I.V., ROSS, M., SEIFERT, F.A. ZUSSMAN, J., AOKI, K. & GOTTARDI, G. (1988): Nomenclature of pyroxenes. Subcommittee on Pyroxenes. Commission on New Minerals and Mineral Names, International Mineralogical Association. *American Mineralogist* **73** 1123–1133.

NESTOLA, F., TRIBAUDINO, M., BOFFA BALARAN, T., LIEBSKE, C. & BRUNO, M. (2007): The crystal structure of pyroxenes along the jadeite-hedenbergite and jadeite-aegirine joins. *American Mineralogist* **92** 1492–1501.

PÉTERDI, B., SZAKMÁNY, Gy., BENDŐ, Zs., KASZTOVSZKY, Zs., T. BIRÓ, K., GIL, G, HARSÁNYI, I., MILE, V., SZILÁGYI, Sz. (2014): Possible provenances of nephrite artefacts found on Hungarian archaeological sites (preliminary results). *Archeometriai Műhely* **11/4** 207–222.

PREWITT, C.T. & BURNHAM, C.W. (1966): The crystal strcture of jadeite, $NaAlSi_2O_6$. *American Mineralogist* **51** 956–975.

RACHINGER, W.A. (1948): A correction for the α1 α2 doublet in the measurement of widths of X-ray diffraction lines. *Journal of Scientific Instruments* **25** 254–255.

SCHUSTER M. & GÖBEL H. (1995): Parallel-beam coupling into channel-cut monochromators

using curved graded multilayers. *J. Phys. D: Applied Physics* **28/A** 270–275.

SMITH, D.C. & GEDRON, F. (1997): Archaeometric Application of the Raman Microprobe to the Non-Destructive Identification of Two Ceremonial Polished Pre-Columbian "Greenstone" Axe-Heads from Mesoamerica. *Journal of Raman Spectroscopy* **28** 731–738.

SZAKMÁNY, Gy. & KASZTOVSZKY, Zs. (2004): Prompt Gamma Activation Analysis, a new method in the archaeological study of polished stone tools and their raw materials: *European Journal of Mineralogy* **16/2** 285–295.

SZAKMÁNY, Gy., T. BIRÓ, K., KRISTÁLY, F., BENDŐ, Zs., KASZTOVSZKY, Zs. & ZAJZON, N.

(2013): Long distance import of polished stone artefacts: HP metamorphites in Hungary. *Archeometriai Műhely* **10/1** 83–92.

WELLS, D.F. & BROWN, C.W. (2009): Processing Powder X-ray Diffraction Patterns with a Fourier Transform Digital Band Pass Filter. *Instrumentation Science & Technology*, **37/1** 89–101.

ZHENG, H. & BAILEY. S.W. (1989): Structures of intergrown triclinic and monoclinic IIb chlorites from Kenya. *Clays and Clay Minerals* **37** 308–318.

ZHOU, Z. & FENG, J. (2010): A petrological and mineralogical comparison between Xinjiang nephrite and Xiuyan nephrite. *Acta Petrologica et Mineralogica* **29/3** 331–340.